J. Fluid Mech. (1987), *vol.* 180, *pp.* 117–145
Printed in Great Britain

Analysis of laminar vortex shedding behind a circular cylinder by computer-aided flow visualization

By B. E. EATON†
Thermophysics Division, National Bureau of Standards, Boulder, CO 80303, USA

(Received 17 February 1986 and in revised form 26 November 1986)

Streamline, streakline, and material-line flow-visualization techniques have been numerically simulated in the vortex-shedding flow field from a finite-element simulation of the two-dimensional Navier–Stokes equations at a Reynolds number of 110. The results have been used (i) to characterize the wake in terms of its critical-point trajectories, and (ii) to verify that the two-dimensional Navier–Stokes model predicts the mechanism of vortex shedding experimentally observed by Gerrard (1978). A technique for determining vorticity balances in the flow field is also presented.

1. Introduction

The study of vortex shedding in the wake of a circular cylinder at low Reynolds number (Re) is important because of the insight it provides into the basic vortex-shedding mechanism. Regardless of whether this mechanism is the same for all values of Re, as has been suggested by some researchers, an understanding of it is certainly a logical step towards understanding the vastly more complicated phenomenon of turbulence.

It will be shown that the two-dimensional Navier–Stokes equations provide a detailed model of the vortex-shedding mechanism at a Reynolds number of 110. Experiments with vortex-shedding flows have shown them to be extremely sensitive to small disturbances, and three-dimensional effects rapidly manifest themselves in the flow field. Consequently the applicability of two-dimensional models has been questioned. The careful flow visualizations of Gerrard (1978) illustrate that the vortices appear in their most regular form immediately behind the cylinder. Further downstream certain regions of the flow field appear in a nearly regular two-dimensional form, while other regions are characterized by the three-dimensional structures called 'knots' by Gerrard.

In this paper, qualitative comparisons are made between the numerical predictions and experimental observations of the vortex-shedding mechanism in the recirculation region immediately behind the cylinder. It is therefore assumed that three-dimensional effects are not influencing the qualitative nature of the vortex-shedding mechanism in this region. A few conclusions about the accuracy of the numerical simulation are based on the comparison with experimental observations further downstream (i.e. more than 2 diameters beyond the rear of the cylinder). It has been assumed in drawing these conclusions that although the observed two-dimensional

† Present address: National Center for Atmospheric Research, P.O. Box 3000, Boulder, CO 80307, USA.

vortex structures are only metastable, they represent the qualitative results that we should expect from our two-dimensional models.

The results typically offered in the literature as verification of the validity of numerical models of vortex-shedding flows are Strouhal number and drag coefficient. However, as pointed out in the review article of Bearman & Graham (1980), numerical models may give values of these parameters that are in good agreement with experimental values, yet give inaccurate predictions of important flow details. The need for a detailed analysis of the flow field has also been recognized by Gresho *et al.* (1984), who showed that while the values of Strouhal number and drag coefficient from their vortex-shedding simulations exhibited agreement with experiment, the details of the vortex-shedding process, as revealed by stream-function plots, appeared to be in disagreement with experimental observations of streaklines. In fact, the details of the wake are the main point of interest if, for example, one is interested in how it interacts with other objects downstream, or in the extent of a chemical reaction occurring in it. Therefore, it is important in verifying two-dimensional models that at least qualitative comparisons of numerical and experimental flow-field structure be made.

Discrete solutions of the Navier–Stokes equations are obtained in the form of velocities and pressures on a set of mesh points as functions of time. It is conceivable that experimental data could be compared with numerical solutions in this form, but this approach is neither efficient nor aesthetic. Flow-visualization techniques seem more promising on both counts because they allow the characteristic flow structures to be identified and quantified by a relatively small number of parameters. A specific example of this concept is the description by Coutanceau & Bouard (1977*a*, *b*) of the steady attached vortices in the wake of a circular cylinder. In that work, streamline patterns and the velocity distribution on the rear flow axis were used to characterize the wake. Similarly, instantaneous streamlines can be applied to the study of periodic wakes as demonstrated by Perry, Chong & Lim (1982). This technique will be used in the present work, and certain characteristics of these streamline representations will be presented quantitatively.

Although a vortex-shedding flow can be characterized by streamlines, a detailed understanding of this complicated phenomenon eludes the observer of instantaneous velocity fields. This is because the recirculation region consists of fluid parcels that have a wide range of residence times, and this essential feature must be studied by tracing the motion of these parcels. The flow-visualization technique that allows us to do this is the tracing of dye lines (or their numerical analogues) in the flow field. In this work two types of dye lines will be considered. The first is a streakline, produced by the continuous injection of dye at a single point. The second, which will be referred to as a material line, is a line of dye placed in the flow field at an instant. The experimental results using dye-tracing techniques are available exclusively as streakline representations.

Much of the work of fitting experimental measurements in vortex-shedding wakes to mathematical models has centred on the use of point-vortex models and variants that account for viscosity. These models lead naturally to the consideration of flow-field vorticity distributions. The final task of this paper will be to present a technique for analysing vorticity distributions, based on using material lines to trace the motion of fluid parcels in the flow field.

2. Solution of the two-dimensional Navier–Stokes model

The two-dimensional Navier–Stokes equations were solved using the Galerkin finite-element method (GFEM). The simulation of vortex-shedding flow past a circular cylinder at $Re = 110$ using GFEM and primitive variables was first done by Gresho, Lee & Sani (1980). The simulation to be analysed here originated from that work and is presented in detail by Eaton (1983). A brief summary of its salient features follows.

The Navier–Stokes equations are written in primitive variables (i.e. x, y components of velocity (u, v), and pressure (p)) with the advection terms in advective form and the viscous terms in stress-divergence form. The incompressibility constraint is enforced via the consistent penalty method advocated by Engelman *et al.* (1982). This technique eliminates the pressures as unknowns from the global system of equations, but requires the use of a discontinuous (C^{-1}) pressure basis for its efficient implementation.

The finite-element mesh, which consists of 196 9-node quadrilateral elements (850 nodes), extends approximately 4 cylinder diameters above, below and upstream from the cylinder, and 15 diameters downstream. A C^0 biquadratic Lagrangian basis is used for the velocity representation, and a C^{-1} linear approximation is used for the pressure (i.e. there are three pressure nodes per element).

The boundary conditions are the result of a sequence of simulations performed to study their effects on the flow around a cylinder. Velocities are set on the upper and lower boundaries of the grid at $(u, v) = (1.0, 0)$; and on the cylinder $(u, v) = (0, 0)$. On the inflow boundary the specified velocity profile is the same as the profile that had resulted from the specification of normal tractions in the original work of Gresho *et al.* (1980). The u-velocity components vary in value from 0.8 to 1.3, with the average value being 1.1 (the Reynolds number of the flow is based on this average velocity). The v-velocity component is set to 0 on the inflow. The outflow conditions resulted from experiments with thermally stratified flows. For the x-momentum equations the normal component of the velocity gradient is set to zero; for the y-momentum equations the tangential stresses are set to zero (in the appropriate weak sense). Additionally, on the bottom outflow boundary element only, the velocity-gradient condition is replaced with a condition setting the normal component of surface traction to zero. This was found to be necessary in order to set a pressure level for the flow.

The initial conditions consist of a solution for a fully developed vortex-shedding flow field from the original simulation done by Gresho. The time-integration scheme is a second-order implicit trapezoid rule which utilizes a second-order explicit Adams–Bashforth predictor to estimate the local time truncation error, and hence has the ability to adjust the timestep size so that the truncation error is controlled to within a specified tolerance. This scheme is modified by taking several initial implicit Euler steps to numerically damp the effects of a spurious pressure transient associated with the penalty method (Sani *et al.* 1981).

The simulation was run for a total of six shedding cycles beyond the initial time, consuming approximately 30 min of CPU time on a CRAY1† at the National Center for Atmospheric Research. The dimensionless period, $\tau V/D$, was 6.8 based on a

† Certain commercial equipment, instruments, or materials are identified in this paper in order to adequately specify the procedure. Such identification does not imply recommendation or endorsement by the National Bureau of Standards, nor does it imply that the materials or equipment identified are necessarily the best available for the purpose.

cylinder diameter D equal to 1, and a characteristic velocity V equal to 1.1. This gives a Strouhal number of 0.15 which is slightly low compared with Gerrard's (1978) estimate of 0.159 ± 0.004. The average drag coefficient was calculated to be 1.31 which agrees with Tritton's (1959) value of 1.26 within his stated experimental error of 6%.

3. Computer-aided flow-visualization techniques

The flow-visualization techniques used in this work depend on the calculation of particle trajectories through the flow field. An integration method designed specifically to work with the finite-element solution is presented in the Appendix. It is a single-step method based on a Taylor series expansion; both first- and second-order schemes are presented.

To compute a particle path through the flow field, one begins by specifying the initial time and position of the particle. The velocity-field data, obtained from the numerical solution, are interpolated to the specified time. Then the quantities required by the integration scheme are evaluated at the particle's position in the flow field. The desired first- or second-order algorithm is used to move the particle a single step, that is, to compute the new position of the particle at the new time $(t+\Delta t)$. Finally, the velocity-field data are 'updated', meaning interpolated to the new time. The methods for constructing the various flow visualizations from the particle trajectories are briefly summarized below.

(i) In the region of the flow where streamlines are desired, the positions of an arbitrary number of origin points are specified. Individual streamlines are constructed from each origin by computing particle trajectories in a steady-state flow field; hence the velocity-field data are interpolated to the desired time and are not updated at the end of each step as the particle trajectories are computed. Also, the partial derivatives of velocity with respect to time are set to zero in the algorithm for computing a single particle move (these derivatives are used only by the second-order scheme).

(ii) A streakline is constructed from a specified origin as follows. First, interpolate the velocity-field data to the initial time, then move a particle one step from the origin point. Next, a new particle is added to the origin, the velocity-field data are updated, and both particles are moved a single step. This procedure is continued, adding a new particle at the origin and updating the velocity field, then moving all the particles a single step. The locus of positions of these particles at a given time represents a streakline. The parameter that varies along a streakline is the residence time of the particles in the flow.

(iii) The path of a material line is determined as follows. The position of each particle that defines the line of interest in the flow field is specified. The number of particles that are required to trace the motion of a 'continuous' line will depend on how severely it is stretched by the flow field, and is determined by trial and error. The material lines presented later in this paper contain particles packed very densely near the cylinder, in order to trace the motion of those parts of lines caught in the recirculation region, and less densely further away. The velocity-field data are interpolated to the initial time, and each particle in the line is moved from its old position to a new one. The velocity field is updated and the process repeated for each step. The particles in a material line all have the same residence time in the flow.

A numerical test was made to indicate the accuracy of the particle-trajectory integration schemes using the streakline computation. A single streakline originating near the upper rear separation point was generated over a period of time equal to

Order of time-integration scheme	Δt used in particle-trajectory calculations			
	$\tau/50$	$\tau/100$	$\tau/200$	$\tau/400$
Δt	2.92	1.73	0.905	0.501
$(\Delta t)^2$	0.657	0.101	0.0277	0.00463

TABLE 1. Maximum error in streakline position

two complete shedding cycles (2τ) using the following time increments in the calculation of the particle trajectories; $\tau/50$, $\tau/100$, $\tau/200$ and $\tau/400$. The positions of 100 particles, whose residence times in the flow field were separated by an interval $\tau/50$, were chosen as the basis for comparison. These positions in each of the streaklines are compared to those from a streakline generated using the second-order scheme with $\Delta t = \tau/800$. In table 1 the maximum error in position from the group of particles defining each streakline is presented. The numbers may be thought of as fractions of the cylinder diameter, which is 1.

The results of this test make two points clear: (i) the errors are behaving in a way consistent with the orders of the schemes, and (ii) for a given level of accuracy, the first-order scheme must use a Δt that is smaller by about a factor of 8. The increase in computational effort required to evaluate the second-order formula, compared to that required for the first-order formula, is about a factor of 2. This increase in computational effort is more than compensated by the increase in accuracy; thus the second-order scheme is the more efficeint of the two. All the streakline and material-line results presented in this paper have been computed using the second-order method with a $\Delta t = \tau/400$. For the streamline results a $\Delta t = \tau/50$ was found to be sufficient because the particle paths required to create the visual image of streamlines are much shorter than for the streaklines.

4. Streamline patterns in the near wake

A sequence of streamline patterns that represents one complete shedding cycle is given in figure 1. These patterns are conveniently described in terms of certain characteristic features which, following Perry *et al.* (1982), will be referred to as critical points. The types of critical point found in two-dimensional incompressible flows are briefly described below.

(i) Inviscid critical points are points of zero velocity in the flow field which occur in two distinct forms: centres, which are points surrounded by closed streamlines; and saddles, which are points where a streamline crosses itself. The loop in a streamline that contains a saddle forms a boundary to the closed streamlines surrounding a centre. At times the area bounded by this loop will be referred to as a vortex, for lack of a better word, although the analogy between these structures and the physical entities we call vortices is limited. This will be explained in more detail later.

(ii) Viscous critical points occur only as saddles, and represent the separation points on the cylinder surface that correspond to points of zero vorticity. These points are seen only from the reference that is stationary with respect to the cylinder.

A streamline that contains either a viscous or an inviscid saddle point is referred to as a separatrix. In figure 1 the separatrices are the heavy lines that have been added

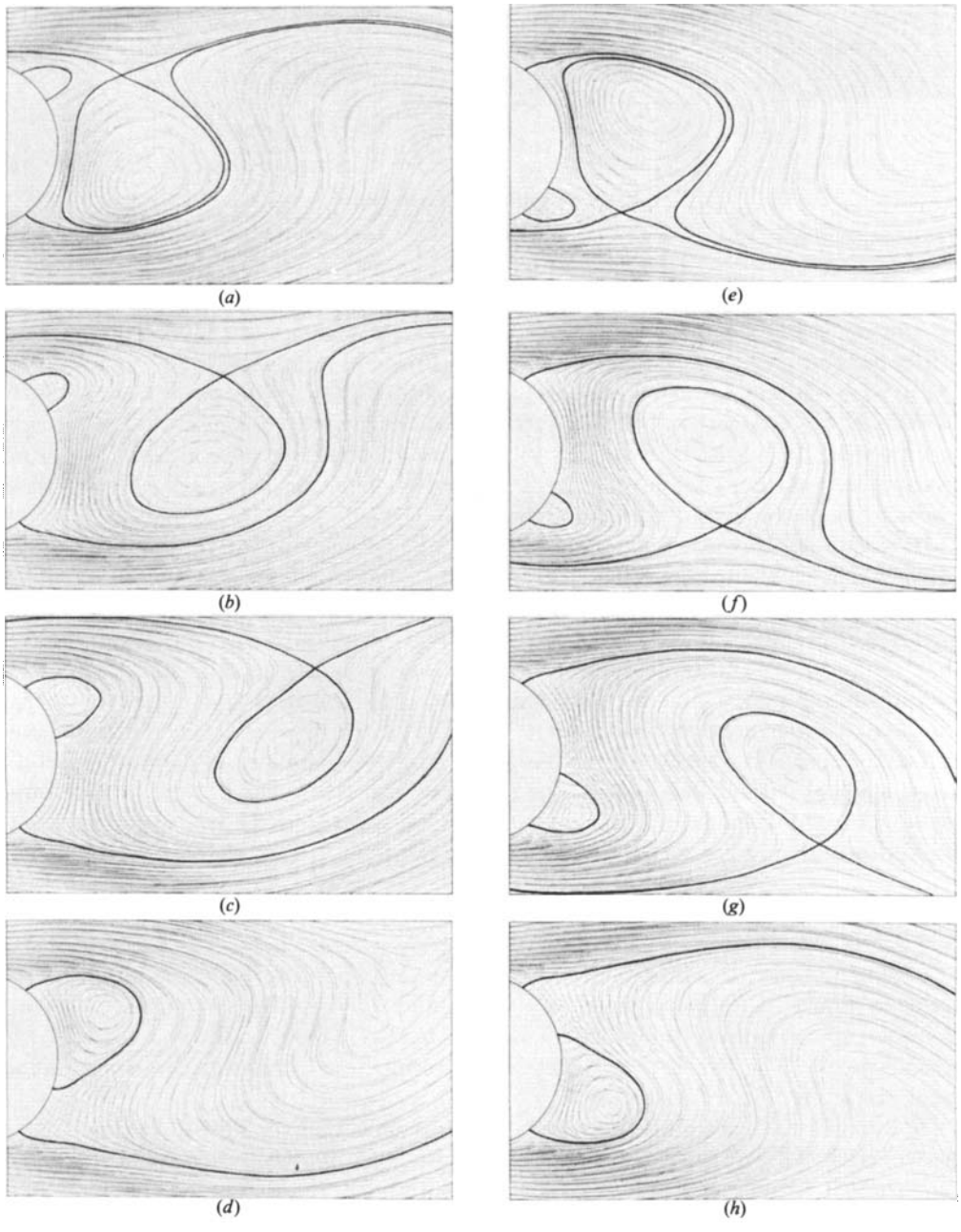

FIGURE 1. Streamline patterns in the near wake separated by an interval of $\tau/8$.

by hand. The reason that the separatrices are not computed using particle trajectories like the other streamlines is that a particle on a separatrix requires an infinite amount of time to reach a saddle point, since the velocity is zero there. Similarly, a particle initially at a saddle point never leaves. Thus, while it is probable that computational techniques could be devised to overcome this difficulty, no effort in that direction was undertaken in the present work.

Drawing the separatrices by hand involves the inevitably biased judgement of

the author, hence a brief description of the accuracy of this procedure is appropriate here. Since no streamline may intersect another one (except at saddle points), the streamlines that are not separatrices act as boundaries to those streamlines that are. The accuracy with which the separatrices may be located thus depends on the density of bounding streamlines. Two parameters determine the streamline density: (i) the density streamline starting points, and (ii) the time interval over which the particles are integrated. By varying these parameters one can focus on a very small region surrounding a saddle and determine the separatrix locations as accurately as required to distinguish the flow patterns in figures 1 and 2.

The sequence of instantaneous streamlines in figure 1 substantiates the main features of the model proposed by Perry *et al.* (1982). Figure 1 (*a–d*) shows a vortex shedding from the bottom of the cylinder while fluid from above the cylinder is drawn down into the recirculation region. The vortex that is forming on the top of the cylinder grows until it reaches the point where it 'breaks off', and the shedding process is repeated in figure 1 (*e–h*).

One of the most prominent features of the streamline pictures is what Perry called the 'instantaneous alleyways', which are the areas where fluid is drawn from above or below the cylinder into the recirculation region. It appears in figure 1 (*a–d*), for example, that the instantaneous alleyway carries fluid from above the cylinder around the forming vortex and down between the shedding vortex and the cylinder to the bottom of the recirculation region, where this fluid is incorporated into the next vortex to be shed. This interpretation was made by Zdravkovich (1969) to explain the results of his experiments which indicated that smoke introduced on one side of the cylinder found its way into vortices shed from the opposite side. However, it will be shown later via dye-line simulations that for the two-dimensional Navier–Stokes simulation being presented here, the fluid brought into the recirculation region from one side of the cylinder remains on that side and is eventually shed in a vortex originating on that side. If the general model shown in figure 1 holds at all Reynolds numbers, as Perry has proposed, then it must also account for flows in which fluid from one side of the wake is entrained into vortices shed from the opposite side, as was observed by Zdravkovich. The point being made here, however, is that the entrainment phenomenon observed by Zdravkovich is not implied by the appearance of instantaneous alleyways.

There is a qualitative discrepancy between the results presented in figure 1 and the model shown in Perry *et al.*'s figure 2 (1982). While figure 1 shows the centre and saddle of a shedding vortex approaching each other and disappearing before a new vortex is shed, Perry *et al.*'s figure 2 shows the centres and saddles of two shed vortices coexisting. The point in the wake where the centre and saddle converge defines the limit of the recirculation region; beyond this point there is no flow back towards the cylinder (in the frame stationary with respect to the cylinder). The implication is that the recirculation region of the flow field in figure 1 is too short. However, a definite conclusion cannot be drawn, since Perry's results were given only in a qualitative form.

The streamline pictures in figure 1 (*a*, *e*) give the impression that the shedding vortex is a large body of fluid (on the order of the size of the cylinder itself). In fact, it will be shown later that only a small fraction of the shedding vortex is composed of fluid that has spent time in the recirculation region. Also, the fact that the centre and saddle of the shedding vortex approach each other and disappear at the downstream limit of the recirculation region does not imply that the vortex has disappeared. If one travels downstream with an appropriate velocity, the centres and

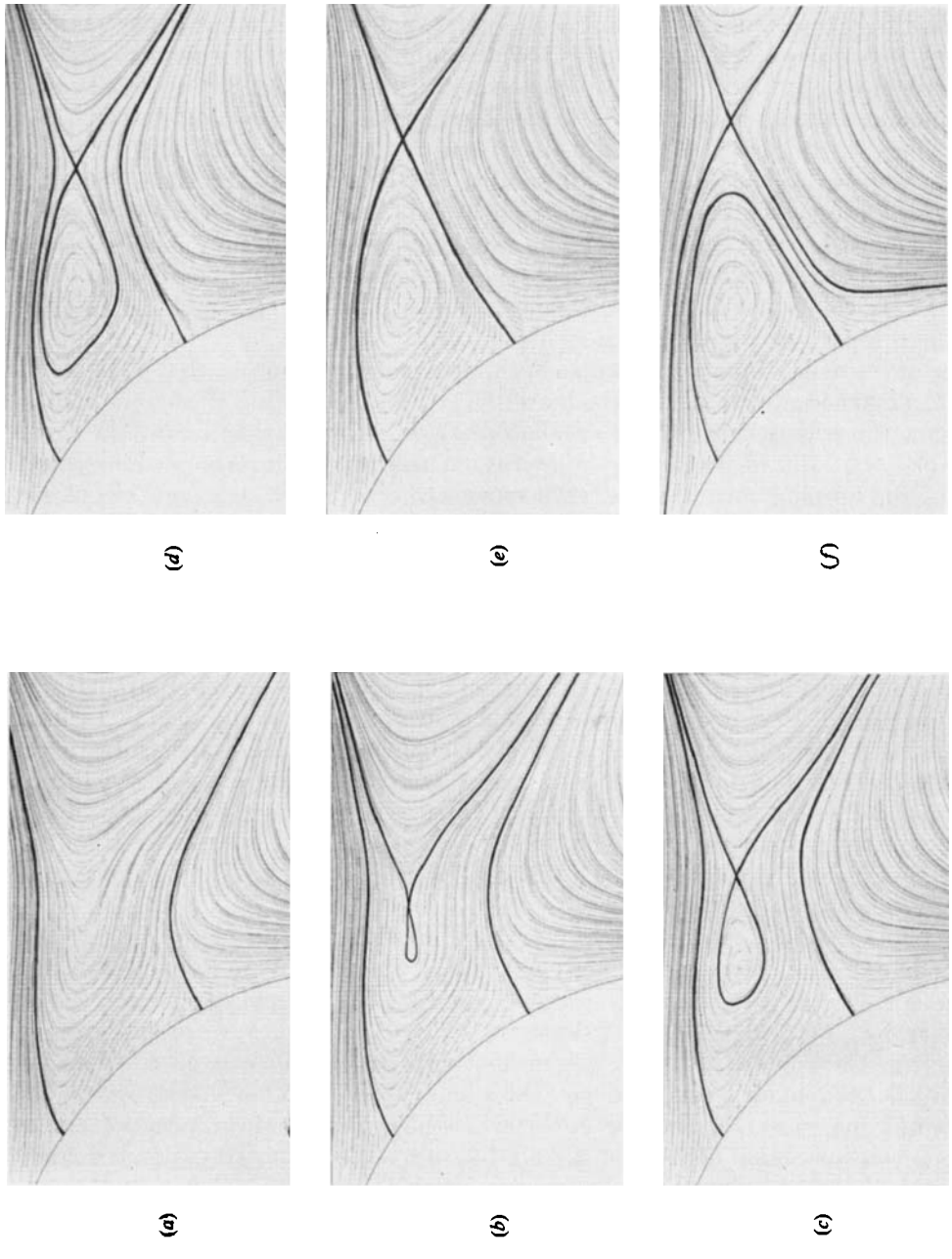

FIGURE 2. Streamlines indicating transition (*e*) from an alleyway drawing fluid into the recirculation region from below the cylinder (*a–d*) to one drawing fluid from above (*f*). Successive plots are separated by an interval of $\tau/124$.

saddles will not disappear. These properties of the instantaneous streamlines illustrate an important point. Although streamlines are very useful for representing the characteristic features of the instantaneous velocity fields, they provide limited insight into the actual flow mechanisms of the recirculation region, which are essentially dynamic in nature.

A point left unclear in the vortex-shedding model proposed by Perry *et al.* is what happens to the separatrices during the transition between having an instantaneous alleyway which draws fluid from above the cylinder to having an alleyway drawing fluid from below, and vice versa. To resolve this question, a small portion of the flow field near the upper portion of the cylinder where the new vortex appears in figure 1 (*a*) was examined more closely. These results are presented in figure 2, where the time increment between successive plots is $\tau/124$. In the context of the streamline sequence that occurs in figure 1, the sequence in figure 2 occurs between figure 1 (*h*) and figure 1 (*a*).

Figure 2 (*a*, *b*) shows that the initiation of a new vortex is due to the growing vortex (with counterclockwise circulation) on the bottom of the cylinder 'pinching' the flow near the upper separation streamline and creating a stagnation point. This mechanism is essentially the same as that observed experimentally by Bouard & Coutanceau (1980) for the formation of certain types of secondary eddies in the recirculation region during the initial stages of flow development behind an impulsively started cylinder. Figure 2 (*b*) shows that a new centre and saddle are formed simultaneously and that the new centre is initially bounded by the separatrix defined by the new saddle, not by one attached to the cylinder. The new vortex grows quickly and the large attached vortex continues to pinch-off the new recirculating region.

The transition from having an alleyway that draws fluid into the recirculation region from below the cylinder, to one that draws fluid from above, is shown in figure 2 (*e*). At the instant of transition, the separatrices look like ones for a closed recirculation region containing two counter-rotating vortices. It appears logical to consider this transition to be the instant when the vortex is shed from the cylinder. This conclusion will be strengthened by the results from the streakline simulations presented later.

5. Critical-point trajectories in the near wake

In the range of Reynolds numbers where the wake contains a steady pair of attached vortices, it is common to characterize this wake by the positions of three types of critical point: the separation points on the rear of the cylinder (viscous saddles), the vortex centres (inviscid centres), and the length of the recirculation region (inviscid saddle). A natural extension of this idea is to consider characterizing the periodic wake in terms of the trajectories of its critical points.

Figure 3 depicts the four characteristic trajectories of inviscid critical points behind the cylinder. The trajectories, which are indicated by a series of dots representing the centre and saddle positions at equally spaced time intervals of $\tau/400$, are superimposed over the finite-element mesh. Where the trajectories appear as solid lines owing to the dots overlapping one another, the critical points are moving more slowly. Time values relative to the time of formation of the top centre and saddle are marked at certain points along the trajectories. The initial positions of the top centre and saddle points are indicated by the arrows pointing in opposite directions and the relative time 0.0. The initial positions of the bottom centre and saddle points

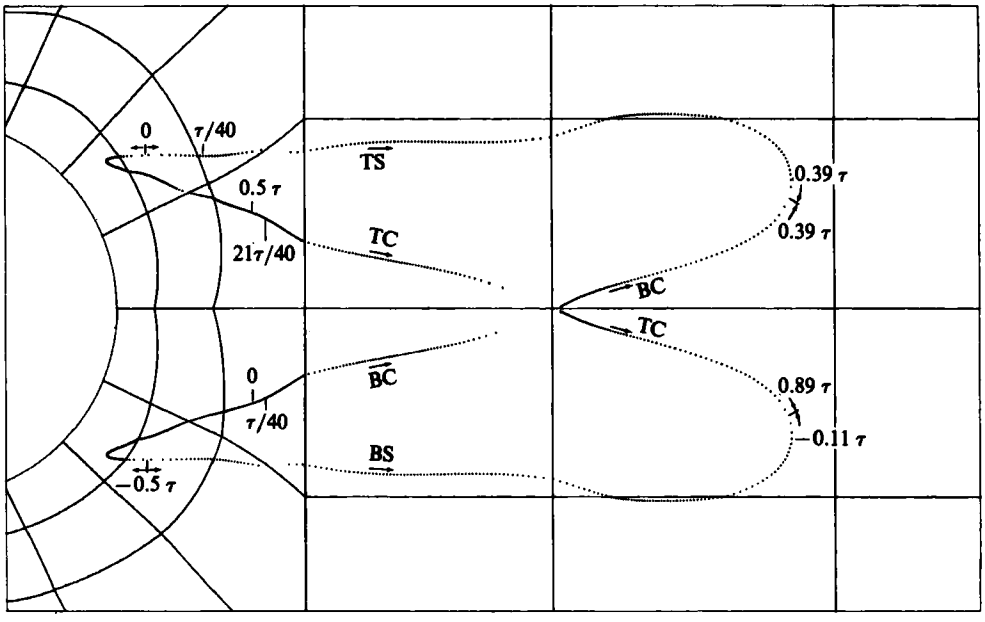

FIGURE 3. Inviscid critical-point trajectories in the near wake. TS, top saddle; TC, top centre; BC, bottom centre; BS, bottom saddle.

are located symmetrically across the wake from the initial positions of the top centre and saddle and are marked with the relative time -0.5τ.

Consider the centre and saddle forming near the upper part of the cylinder at $t = 0$. At this time a vortex is about to be shed from the bottom of the cylinder as was shown in figure 2. Figure 2 (*b–d*) shows that the separatrix defined by the new saddle initially bounds the new centre, but after a short time (approximately $\tau/40$) this separatrix surrounds the vortex that is shedding from the bottom of the cylinder. The position of the bottom centre at the time that the vortex sheds is at the spot marked $\tau/40$; it originated one half-period earlier than the top saddle that attaches to it. The centre and saddle of the shedding vortex approach each other as they move downstream, meeting at a point that defines the limit of the recirculation region. The disappearance of the centre and saddle of the shedding vortex occurs at $t = 0.39\tau$, which is before the next vortex is shed at $t = 21\tau/40$, as was pointed out in the discussion of figure 1. In this simulation, the length of the recirculation region is 1.8 diameters beyond the rear of the cylinder.

The centre of the new vortex near the top of the cylinder initially moves towards the cylinder, then slowly away as it grows. At $t = 0.5\tau$, the next centre and saddle form near the bottom of the cylinder, and at $t = 21\tau/40$, the new saddle attaches to the top centre and the vortex sheds from the top of the cylinder.

To summarize, a new centre spends one-half of the cycle 'attached' to the cylinder, then attaches to a saddle that originates on the opposite side, and moves downstream for a time of 0.39τ until the centre and saddle converge.

In an attempt to further quantify the critical-point trajectories, the vorticity and velocity of the top centre point are given in figure 4 as a function of time. The most striking feature of both of these plots is the magnitude of the jumps, which are due in both cases to discontinuities in the spatial derivatives of the velocity field at the

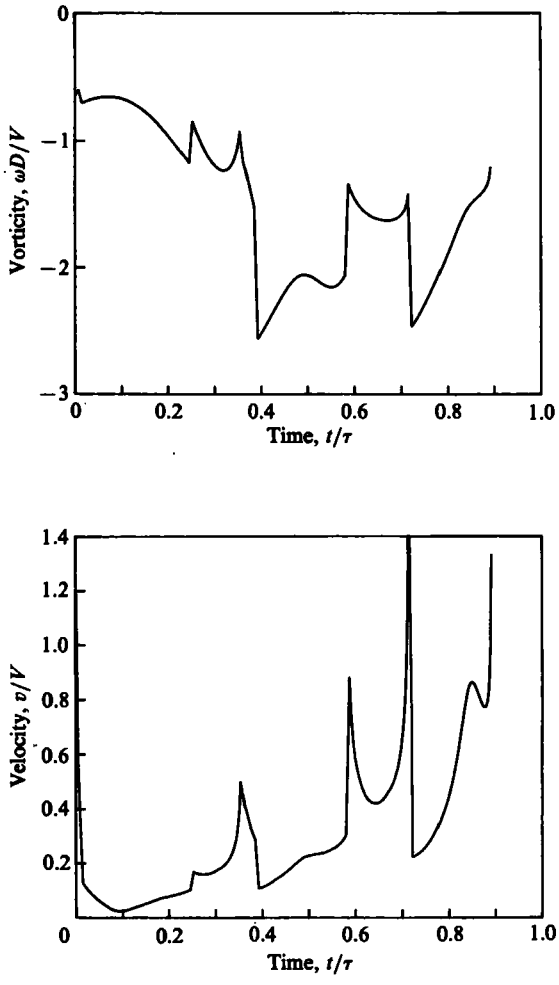

FIGURE 4. Velocity (v) and vorticity (ω) along an inviscid centre trajectory. Quantities are made dimensionless using the characteristic velocity $V = 1.1$, diameter $D = 1.0$, and period $\tau = 6.2$.

element boundaries. The jumps in velocity can also be discerned in figure 3, where the trajectories cross element boundaries, as indicated by the abrupt changes in spacing between the points near these boundaries. A particularly large jump occurs where the two centre trajectories cross. This corresponds to the peak that is off-scale on the velocity plot in figure 4. The fact that the discontinuities are of the same magnitude as the total variations along the trajectories makes it difficult to extract useful information from these plots.

The size of the discontinuities in the plots of figure 4 indicates that the finite-element mesh used for this simulation is too coarse to resolve accurately the details of the critical-point trajectories. These trajectories appear to be sensitive indicators of the accuracy with which the Navier–Stokes equations are solved. However, from the point of view of applications, as will be shown shortly, the inaccuracies in these critical-point trajectories do not seem to have a serious effect on the qualitative patterns of fluid flow.

In figure 5 the trajectories of the viscous critical points (separation and reattach-

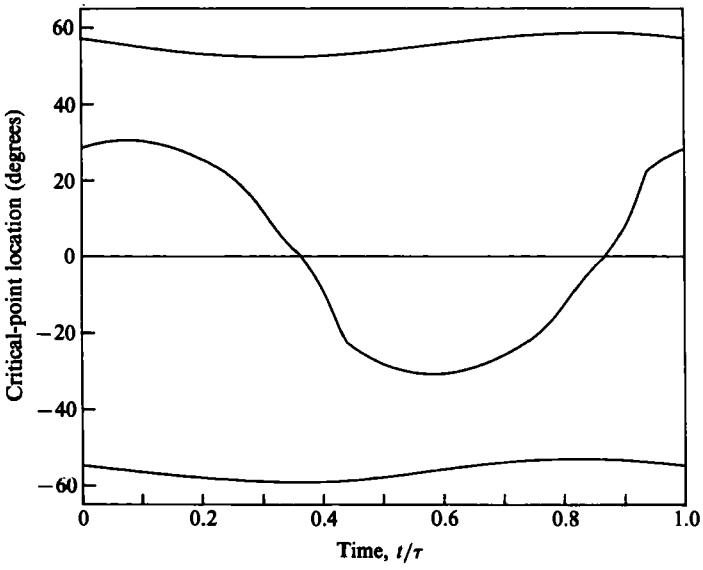

FIGURE 5. Separation- and reattachment-point trajectories on the rear of the cylinder.

ment points) on the rear of the cylinder are given for a full shedding cycle. Time zero represents the time of a new centre/saddle formation near the top of the cylinder. The position of a point is represented by its angle (in degrees) from the rear centre position on the cylinder. As with the inviscid critical points, the velocity of the middle separation point along the rear of the cylinder contains discontinuities at element boundaries. These discontinuities only appear on the middle curve, because the trajectories of the upper and lower separation points remain within a single element.

6. Streaklines

Although the instantaneous streamlines provide a convenient means of characterizing the wake, they provide only limited insight into the dynamics of the recirculation region responsible for the formation of vortices. The primary method used to understand the vortex formation process is to trace the motion of fluid parcels, normally by the generation of streaklines. In this section streaklines which have been generated for the two-dimensional Navier–Stokes solution are compared to the experimental results of Gerrard (1978) and Zdravkovich (1969).

Figure 6 shows a set of twelve streaklines, ten of which originate outside the rear separation points, while the two innermost lines originate just inside the rear separation points. The streaklines are shown on the full computational grid downstream from the cylinder at a time corresponding to the transition from having an alleyway that draws fluid into the recirculation region from below the cylinder, to one that draws fluid from above, as shown in figure 2(*e*). To aid the interpretation of figure 6, refer to figure 7, in which four of the streaklines originating above the cylinder and the streakline originating near the upper stagnation point are shown separately. The origin points for the streaklines in figure 7(*a–d*) are 1, $\frac{1}{2}$, $\frac{1}{4}$ and $\frac{1}{8}$ diameters above the top of the cylinder respectively.

In discussing the streaklines in figure 7, advantage will be taken of the periodic nature of vortex shedding to show, on the plot of a single streakline, how particular

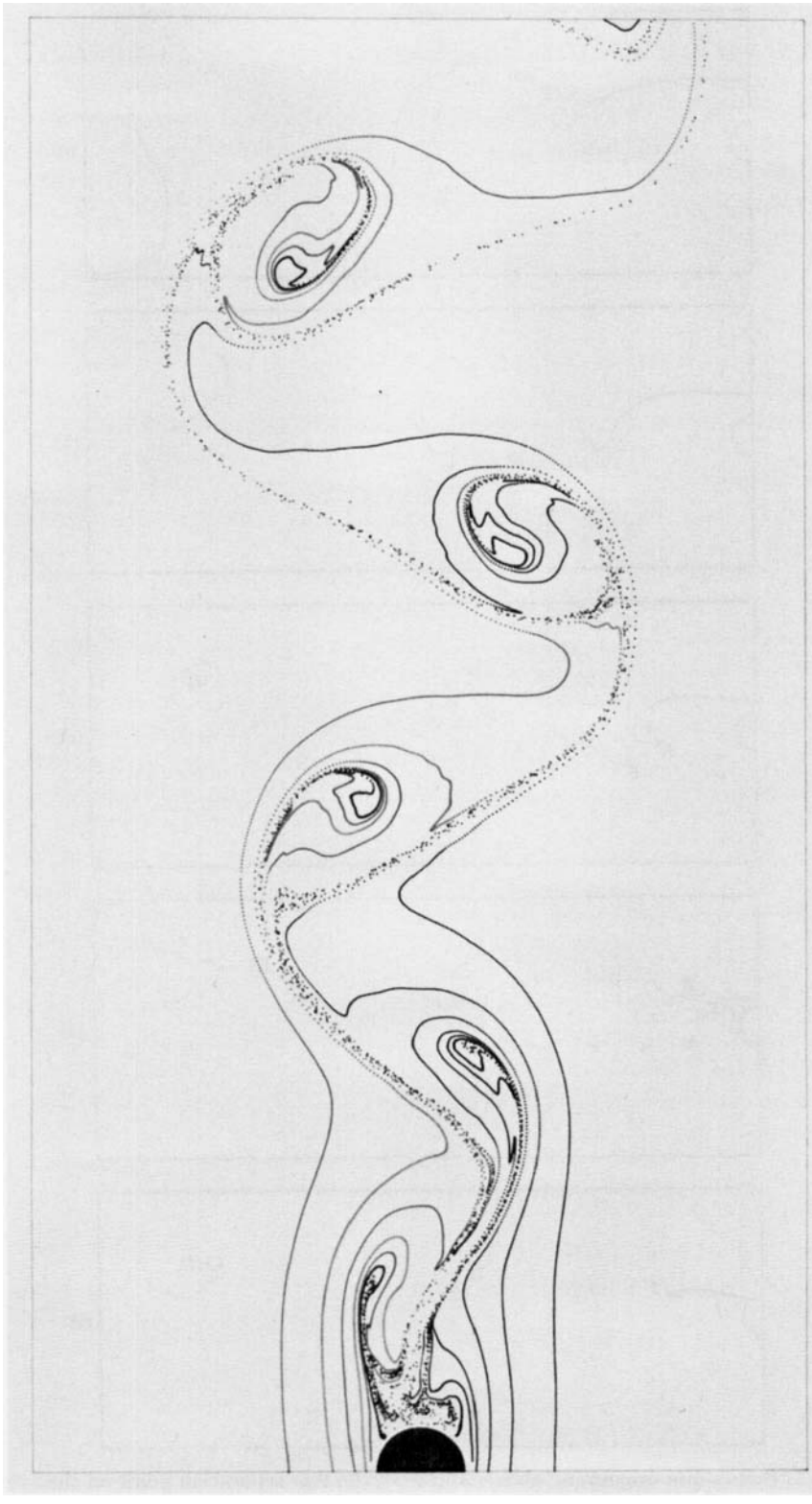

FIGURE 6. Streaklines in the wake of a circular cylinder at $Re = 110$.

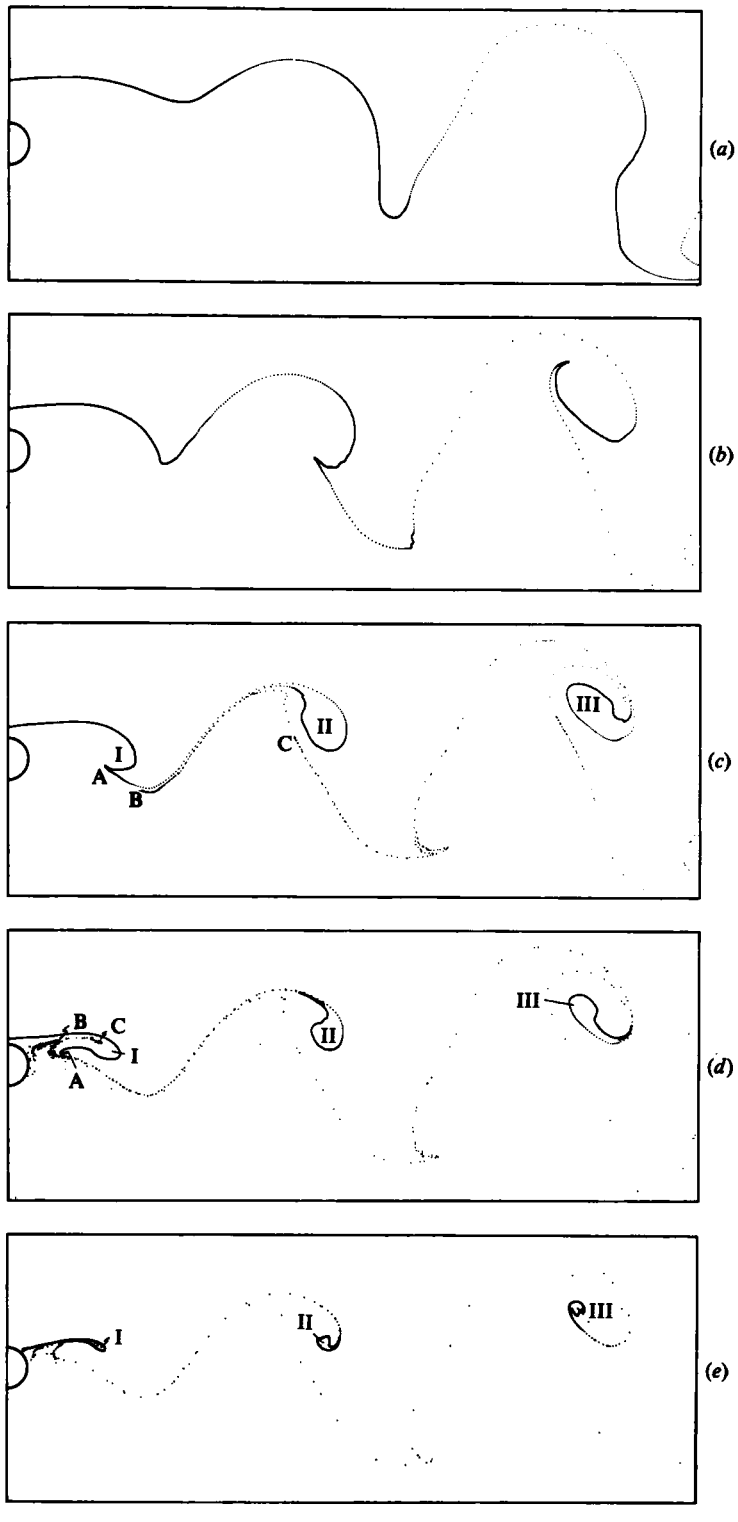

FIGURE 7. Streaklines originating above, and from the rear separation point on the cylinder. The symbols A, B, C, I, II and III are explained in the text.

features of the streakline move from one period to the next. The top three streaklines are not caught in the recirculation region; however, figure 7(*c*) shows that the streakline originating $\frac{1}{4}$ diameter above the cylinder is very close to bounding those streaklines that are caught in it from those that are not. The point marked A in this figure moves only a small distance to the point marked B during a single period in the flow, then to the point marked C during the next period. During this same time the centre of the vortex, marked by the symbol I, moves to the position marked II during the first period, then to the position marked III in the following peiod. The relative motion between the points I and A, II and B, and III and C results in severe stretching of the streakline. The particles near A have approximately the same residence times (within, say, one half-period) as the particles composing the loop in the streakline around the vortex marked I. This same relationship holds between the point B and the vortex II, and between C and vortex III. Thus the stretching of the streakline indicates a wide range of residence times for the particles in certain regions of the wake.

In figure 7(*d*), parts of the streakline are caught in the recirculation region. The relationships between the points marked A and I, B and II, and C and III in this figure are analogous to the relationships between the points similarly marked in figure 7(*c*). This implies the following: the particles near B have a residence time approximately equal to those that are being carried by the vortex marked II, and similarly for C and vortex III. The particles near C will be carried downstream by the vortex that is shedding (marked I), and the particles near B will be carried downstream by the next vortex to shed from the top.

Figure 7(*e*) shows a streakline originating just inside the separation line. This streakline acts as a boundary between the fluid being 'injected' into the wake from the recirculation region and the fluid that originates outside the separation line and passes downstream without spending time in the recirculation region. The sense in which this streakline is considered 'bounding' is the following. A superposition of the streaklines, as in figure 6, shows that the particles near the points B and C in figure 7(*d*) are injected into the wake inside the loops of the bounding streakline of figure 7(*e*). Thus, the material inside the loops of the bounding streakline has spent time in the recirculation region. On the other hand, the fluid outside this loop as it travels downstream did not spend time in the recirculation region. Consider, for example, the vortex marked II in figure 7(*c–e*). The loop formed by the bounding streakline of figure 7(*e*) contains fluid that spent time in the recirculation region. The loops formed by streaklines that originated outside the separation line, as represented in figure 7(*c*, *d*), are composed of particles that have not spent time in the recirculation region.

The preceding observations of the bounding streakline motivate the following physical description of a 'vortex core'. The vortex core could be considered as that area defined by the loops in the bounding streakline; i.e. the fluid injected into the wake from the recirculation region. For a vortex core defined in this way, it seems logical to correlate the initiation of the vortex-shedding process with the initiation of the process by which the vortex core is injected into the wake. This correlation is supported by figure 6, which represents the time of transition from a lower alleyway to an upper one. It was previously suggested that this transition represents the instant that the bottom vortex is shed into the wake. Figure 6 shows that this time also corresponds to the initiation of a bulge in the lower bounding streakline, indicating that the vortex core is being injected into the wake.

The amount of fluid carried downstream by a vortex core represents the amount

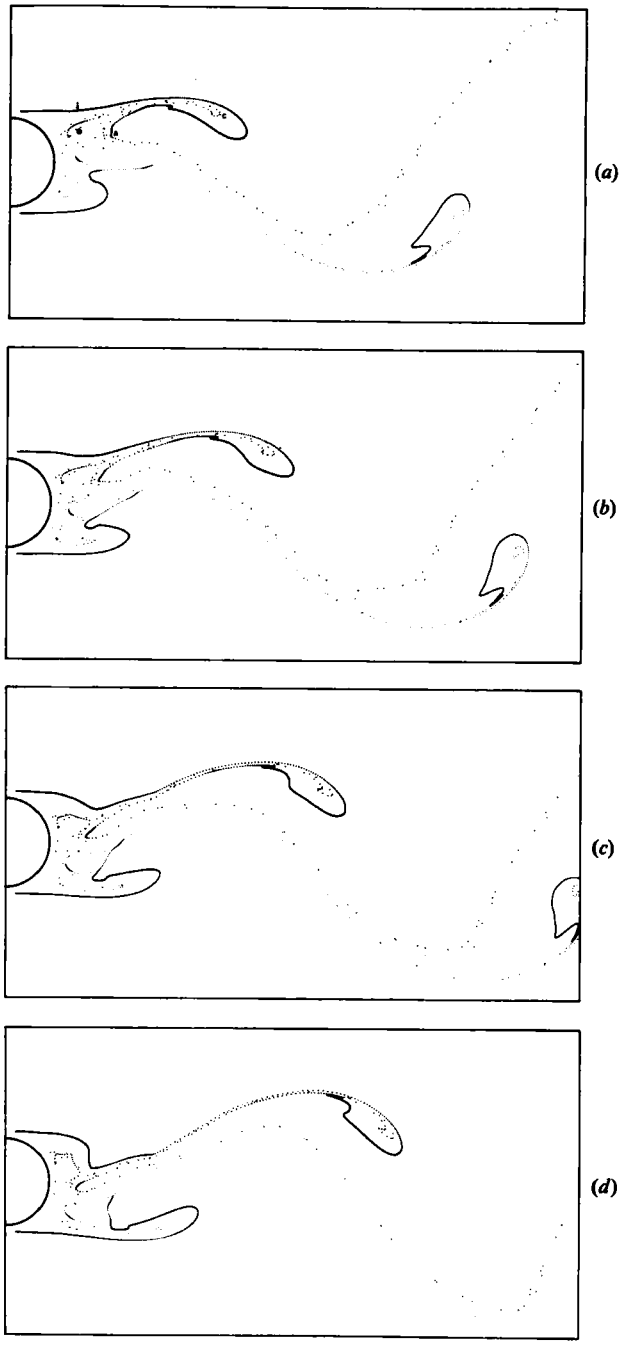

FIGURE 8(*a–d*). For caption see facing page.

of material that must be taken into the recirculation region during each half-period in order to maintain the mass balance. Observation of the streakline presented in figure 7(*d*) indicates that the main part of the fluid in the recirculation region was flowing past the cylinder, within $\frac{1}{4}$ of a cylinder diameter, two cycles earlier. During the first cycle after flowing past the top of the cylinder, fluid is pulled down into the

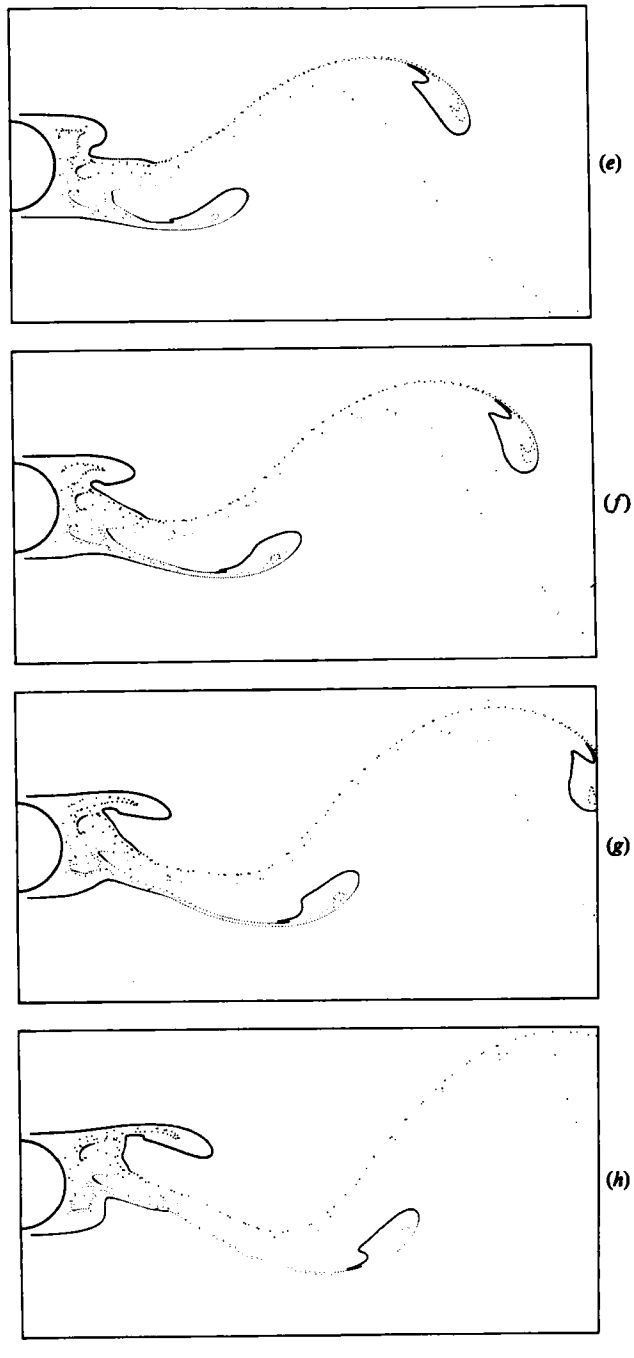

FIGURE 8. Streakline sequence covering one shedding cycle. Symbols are explained in the text.

region near the point marked A. Part of this fluid will spend the next cycle in the recirculation region advancing towards B, and during the following cycle will advance to C to be injected into the wake as the core of vortex I.

In order to illustrate the fluid motion behind the cylinder for a single shedding cycle, figure 8 presents a sequence of streakline plots separated by intervals of $\tau/8$.

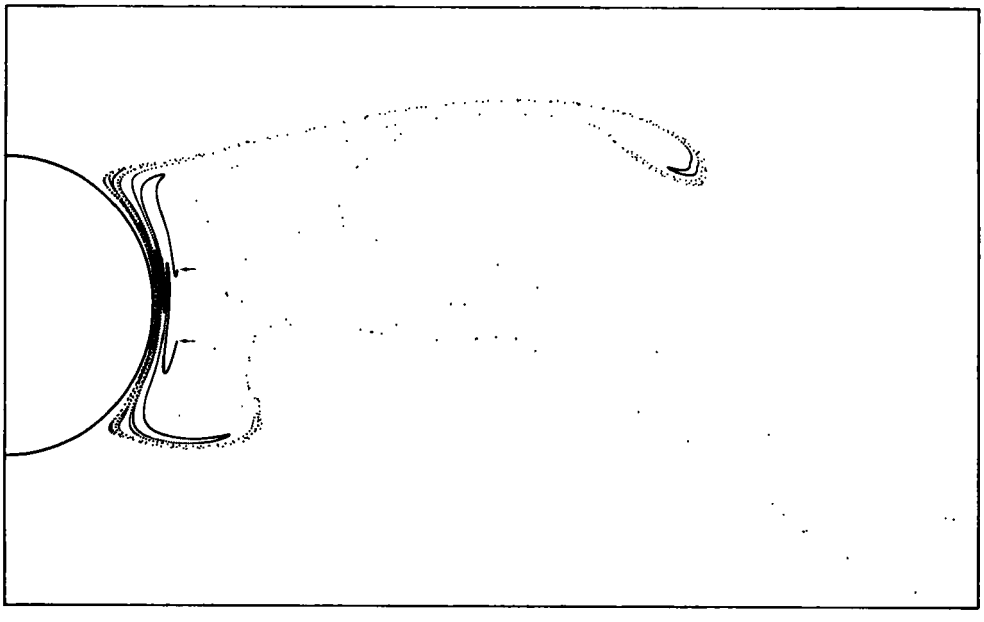

FIGURE 9. Streaklines originating near the rear of the cylinder. Arrows indicate streakline origins.

The times represented correspond exactly to those for which the instantaneous streamlines were presented in figure 1 (the portion of the flow field shown, however, is not the same). In figure 8 (*a–d*) a vortex is shedding from the bottom of the cylinder and the instantaneous alleyway is bringing fluid from above the cylinder into the recirculation region. As pointed out by Perry *et al.* (1982) the formation of an instantaneous alleyway corresponds to the initial indentation that forms in a streakline, indicated in figure 8 (*a*) by the arrow. At the same time that the new fluid is being brought down behind the cylinder, the fluid in the region marked A in figure 8 (*a*), which had been brought behind the cylinder in the previous cycle, moves in towards the cylinder. If the dye line just to the left of A is followed through the sequence of figures 8 (*a–h*), then after a single period (i.e. upon returning to figure 8 (*a*) in the sequence) it will be in the position marked B. Similarly, by following the dye line from the position marked B through the sequence one observes that in a single period these particles will move to the position marked C. Thus the particles in the position marked B in figure 8 (*a*) will be shed in the vortex that is just beginning to form on the top of the cylinder in that figure.

In the flow-visualization experiments performed by Gerrard (1978) dye was applied to the cylinder between the rear separation points. The following observations were made by him. At Reynolds numbers of less than 100, dye washed from the cylinder accumulates in the recirculation region, indicating that the fluid there is circulating for many periods. At Reynolds numbers greater than 100, however, the dye was not observed to accumulate in the recirculation region, but rather was 'scavenged' into the shedding vortices. Single dye filaments were not observed to remain behind the cylinder for more than one period of oscillation.

The absence of an accumulation of dye behind the cylinder in the experimental observations of Gerrard (1978) at *Re* greater than 100 indicates that the recirculation region is composed mainly of fluid that originated outside the separation lines (i.e.

undyed fluid), and is thus in agreement with the flow mechanism illustrated by the streaklines in figures 6–8. To further illustrate the agreement between the predictions of the two-dimensional Navier–Stokes model and Gerrard's experimental observations, a pair of streaklines were generated that originate near the rear of the cylinder, thus providing a more direct comparison with his specific experimental techniques. These streaklines are shown in figure 9 at the same time as the streaklines in figure 6; arrows indicate the streakline origins. The particles in these streaklines accumulate in a narrow region close behind the cylinder and are injected into the wake along the separation lines. Since the velocities immediately behind the cylinder are very small, the particles remain there for many cycles before working their way to the separation points. The main part of the recirculation region contains very few particles that originated along the rear of the cylinder and were injected into the wake along the separation lines. These observations are in agreement with Gerrard.

In comparing figure 7 with the experimental results of Zdravkovich (1969), in particular his figure 3, several observations can be made. For the streaklines that are introduced far enough above the cylinder not to be caught in the recirculation region, Zdravkovich notes that as they interact with the wake downstream they concentrate around the vortices that have been shed from both sides of the cylinder. This phenomenon is also predicted by the numerical model as shown in figure 7 (*a*, *b*), although these streaklines appear to concentrate around vortices shed from the top of the cylinder as opposed to those shed from the bottom as reported by Zdravkovich. Zdravkovich's figure 3 (*c*) shows a streakline that is caught up in the recirculation region. The vortices downstream all show an absence of smoke in their centres; a result that he concluded was due to the incorporation of fluid from below the cylinder into the vortices shed from the top. This observation cannot be reconciled with the results from the two-dimensional Navier–Stokes model presented here. As shown in figure 7 (*d*, *e*), the fluid from above the cylinder is never observed in vortices shed from the opposite side of the wake. As a point of clarification, the reason that the vortices marked II and III in figure 7 (*d*, *e*) appear to have empty centres is a start-up effect of the streakline computation. It takes several cycles for the parts of the streakline that are caught in the recirculation region to be taken into a shedding vortex. The particles at the spot marked C are the first to be shed; two periods later, all the vortices would contain particles injected from the recirculation region.

While the prediction of the numerical model that fluid originating on one side of the wake stays on that side contradicts the experimental results of Zdravkovich, it agrees with the experimental results of Gerrard (1978). Since Gerrard's experiments were performed in a towing tank in which great efforts were made to minimize disturbances, it is possible that the results of Zdravkovich are related to the disturbance level of his wind tunnel. The admonition of Berger & Wille (1972) is worth repeating; experimental results in this field should be published with clear statements on the turbulence level of the flow system used.

There is a discrepancy between the experimental results of Gerrard and the model being examined which is most easily seen by comparing figure 7 (*e*) with Gerrard's figure 21, which shows the vortex cores, shed from the top of the cylinder, moving along a line that is approximately even with the top of the cylinder. Figure 7 (*e*) on the other hand shows that the vortex core that is about to leave the grid has risen almost a full cylinder diameter above that level. This result indicates problems with the outflow boundary conditions imposed by the numerical solution. Another potential problem with the numerical solution is indicated by figure 6. Since the wake downstream from the cylinder is non-uniform over a large width, the conditions set

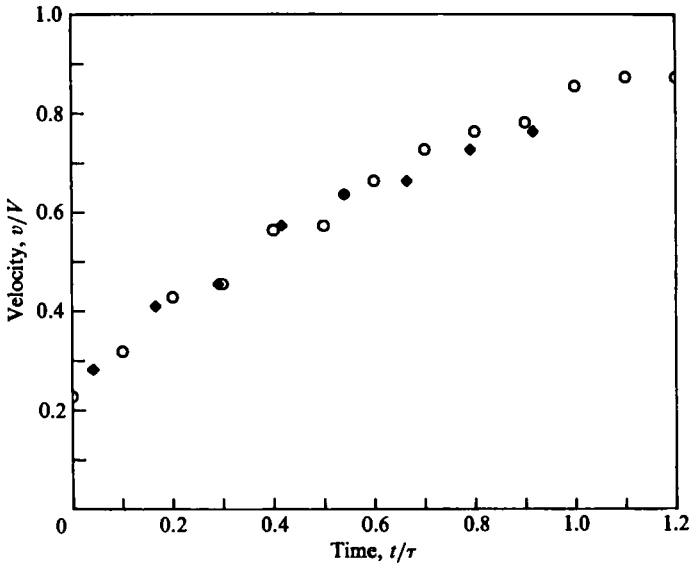

FIGURE 10. Velocity of a shedding vortex: ○, data set at intervals of $\tau/10$; ◆, data set corresponding to the times in the sequence of figure 8.

on the upper and lower boundaries, which are designed to be infinity conditions, are probably too restrictive.

A quantitative result that can be obtained from the streakline representation is that for the velocity of the vortex as it sheds from the cylinder. The vortex velocities were obtained graphically from streakline plots in the following way. Two streaklines, having the same origin as those in figure 8 and separated by an interval of $\tau/200$, are plotted together. Lines parallel to the y-axis are drawn tangent to the loops formed by the streaklines surrounding the vortex cores. The distance between these lines is divided by the interval to obtain the vortex velocities, which are given in figure 10; the time $t = 0$ corresponds to the streamline configuration shown in figure 2(*e*). The scatter of the data in figure 10 is an indication of the imprecision of the graphical technique. Also, no consideration has been given to the fact that the streakline loop used to measure the vortex velocity is rotating as it translates downstream. The time over which the vortex accelerates is approximately one period, which is in agreement with Gerrard's interpretation of the rather scattered experimental results for this quantity. The steady velocity attained by a shedding vortex is approximately 90% of the average inflow velocity.

A claim has been made in this paper that the instantaneous streamlines are insufficient to explain the dynamics of the recirculation region. Figures 11 and 12 are presented to substantiate this claim and, in so doing, to clarify the complex relationship between streamlines and streaklines. The streaklines in these figures are identical with those in figure 8. The streamlines in figure 11 are relative to an observer who is stationary with respect to the cylinder. In figure 12 the streamlines are relative to an observer who is moving with the vortex that is shedding from the bottom of the cylinder; hence the relative velocity used to compute the streamlines in figure 12 is different for each of the individual plots (these velocities may be found in figure 10). In discussing figures 11 and 12, the term 'centre' will be used to describe a critical point in the instantaneous streamline representations and the term 'vortex core' will

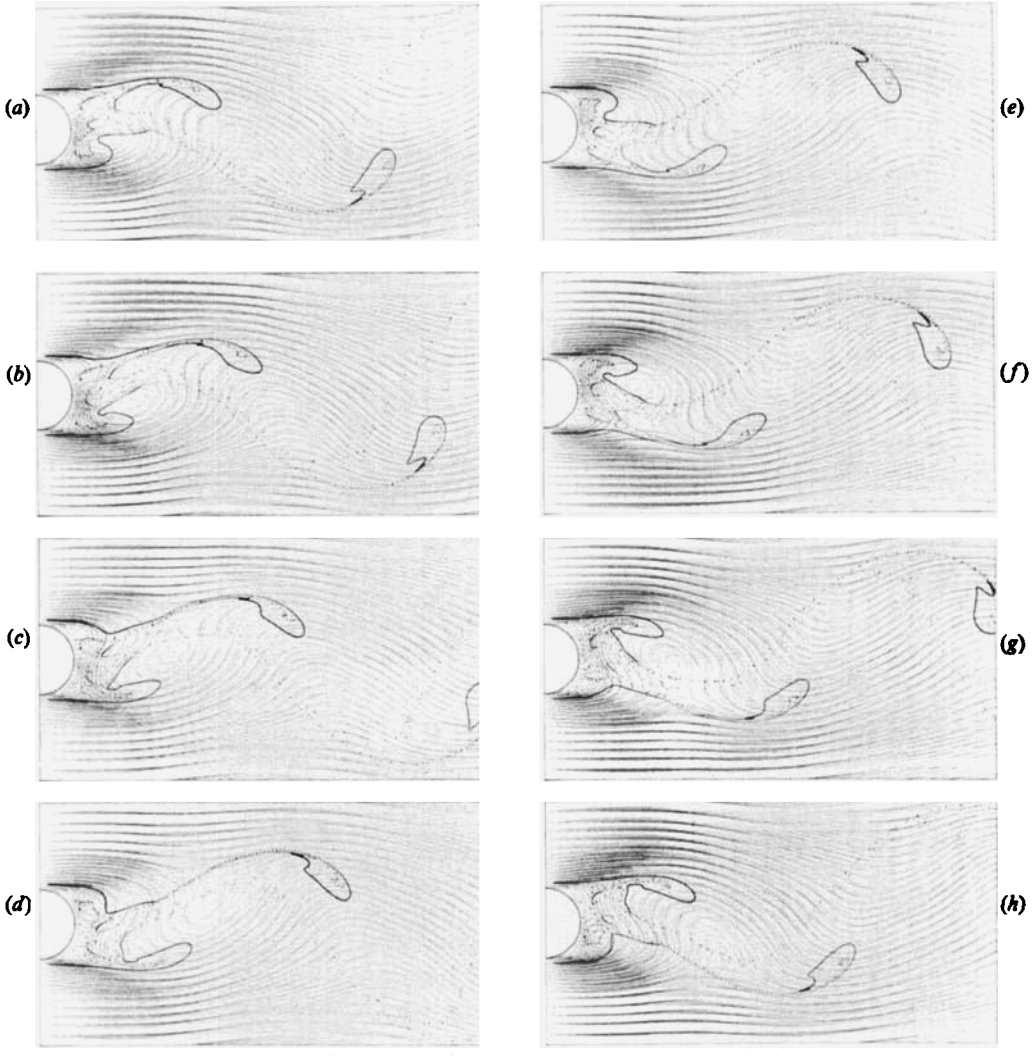

FIGURE 11. Streakline–streamline sequence covering one shedding cycle. Observer is stationary with respect to the cylinder.

be used in the sense described above. Thus the positions of the vortex cores are roughly indicated by the particles from the recirculation region that are injected into the loops formed by the streaklines.

The meaning of the statement that the instantaneous streamlines do not represent the dynamics of the recirculation region is, more precisely, the following. First, during a half-period in which an alleyway is bringing fluid from one side of the cylinder, say the top, into the recirculation region, one cannot determine without tracing the motion of particles the extent to which that part of the fluid in the recirculation region, which originated on the top side of the cylinder, travels towards the bottom. Secondly, the centres do not follow the trajectories of the vortex cores; this is clear in figure 11. Returning to the first point, in figure 11 (*a–d*), for example, the alleyway is bringing fluid from above the cylinder into the recirculation region. The part of

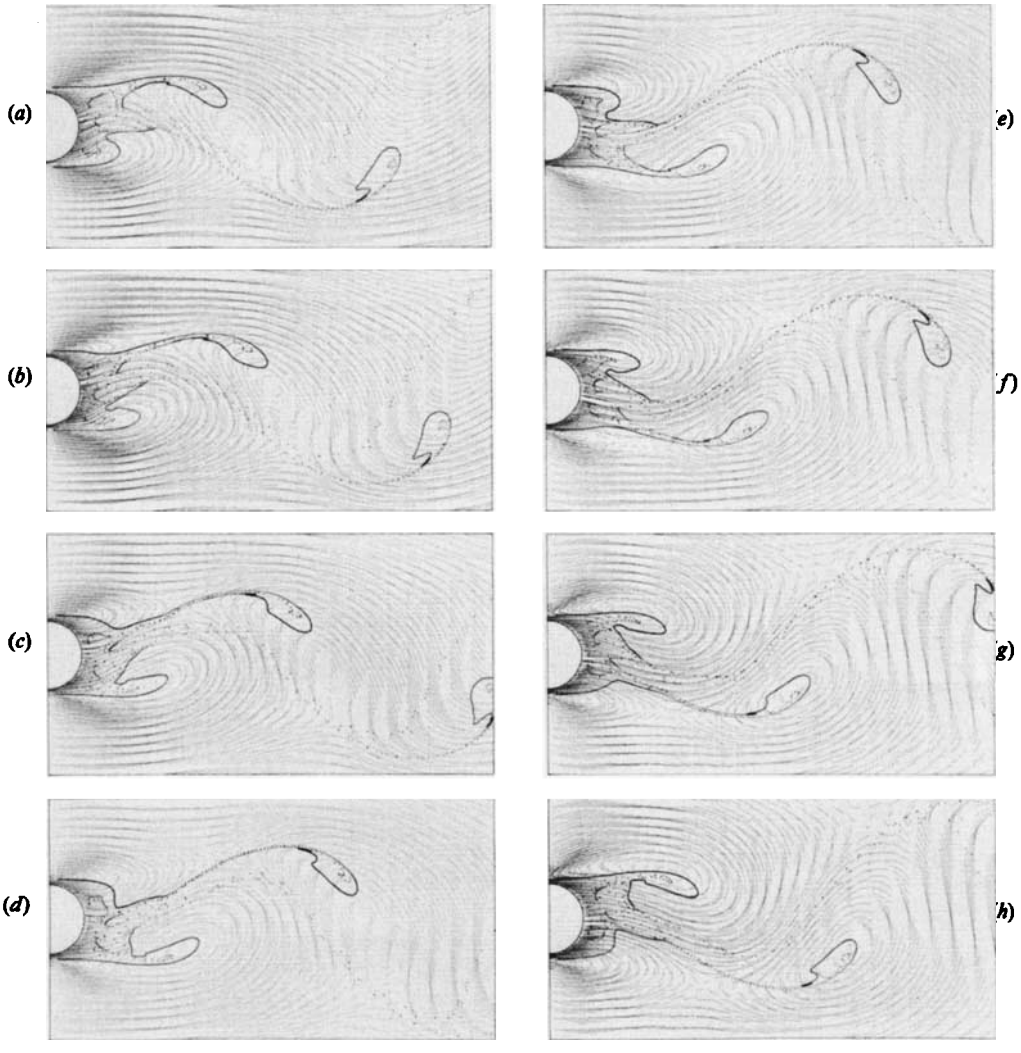

FIGURE 12. Streakline–streamline sequence covering one shedding cycle. Observer is moving with the vortex that is beginning to shed from the bottom of the cylinder in (*a*).

the recirculation region containing particles that originated above the cylinder is seen to have a lower boundary that moves from a position approximately $\frac{1}{4}$ of a cylinder diameter above the centreline in figure 11(*a*) to a position approximately $\frac{1}{4}$ of a cylinder diameter below the centreline in figure 11(*e*). Thus the existence of the alleyways does not imply that fluid from one side of the cylinder is carried to the other side and incorporated into vortices shed from there.

The fact that the centres do not correspond to the vortex cores can be remedied to a certain extent by computing the streamlines in a frame of reference that moves with the vortex. However, within 10 cylinder diameters of the rear of the cylinder, the vortices are all travelling at different speeds, implying that only one centre and vortex core can be matched; this is apparent in figure 12.

An idea which was investigated during the course of this work was to define a vortex by making use of the separatrices in the streamline representations computed in the

frame of the moving vortex. In the proposed scheme, the vortex would consist of the fluid bounded by the chosen separatrix, with its strength determined by the total vorticity of this body of fluid. This approach was not considered successful for the following reason. It is intuitive that the vortex should gain in strength as it grows behind the cylinder, and decrease in strength because of dissipative processes after it is shed. No separatrix was found that had these properties.

7. Vorticity distribution in the wake

A natural way to describe the most characteristic features of the wake is in terms of its vorticity distribution. Since the classic description by von Kármán of the periodic wake in terms of point vortices, most wake models have been based on this idea. The most important modification to this model has been the incorporation of viscous effects. An excellent overview of the fundamental assumptions embodied in the original wake models is contained in Birkhoff & Zarantonello (1957). The fitting of models that account for viscous effects in cylinder wakes is described by Bloor & Gerrard (1966).

In fitting a vortex model to experimental results, one begins by assuming that the vorticity generated at the surface of the cylinder should be present in the vortices. The model is fitted by adjusting parameters to minimize some measure of the differences between the experimental velocity meaurements and the model values at specific points in the flow field. The vortex strength is then obtained from the model and is multiplied by the shedding frequency to determine the rate at which vorticity is carried away by the wake. The rate of vorticity generation by the cylinder is determined by velocity measurements in conjunction with boundary-layer theory. The difference between the vorticity generated and that contained in the vortices is assumed to have been 'cancelled' by diffusion into vorticity of the opposite sign (i.e. vorticity generated on opposite sides of the cylinder is oppositely signed). Research using these techniques on low-Reynolds-number flows has shown the vorticity lost by cancellation to be about 60 % of the total generated by the cylinder (Berger & Wille 1972). An implication of such a large vorticity loss is that fluid from one side of the cylinder is entrained into the vortex forming on the other side. Since this mechanism is inconsistent with both the predictions of the two-dimensional Navier–Stokes model and the experimental observations of Gerrard, the applicability of this type of wake model to low-Reynolds-number flows may reasonably be questioned.

The purpose of this section is to present a more general way of performing a vorticity balance in the wake. The technique is based on following material elements of fluid by integrating material lines through the flow field. A vorticity-balance equation, derived from the linear momentum equation, tells us that the rate of change of vorticity in a material volume is due solely to diffusion across the boundary of the volume. By appropriately choosing a material element, the diffusion across certain boundaries can be neglected and an estimate made of the vorticity lost by diffusion into the wake region.

The material element on which the vorticity balance is performed is shown in figure 13(*a*). This element consists of all the fluid that flowed past the line segment AB during one shedding period. It was constructed by placing a material line, which corresponds initially to the segment AB, in the flow field at a given time and integrating it for a period to generate the line AC. The point A is a rear separation point on the cylinder, hence it does not move noticeably. The point B is far enough from the cylinder to be outside the vorticity-carrying fluid; it moves linearly to the

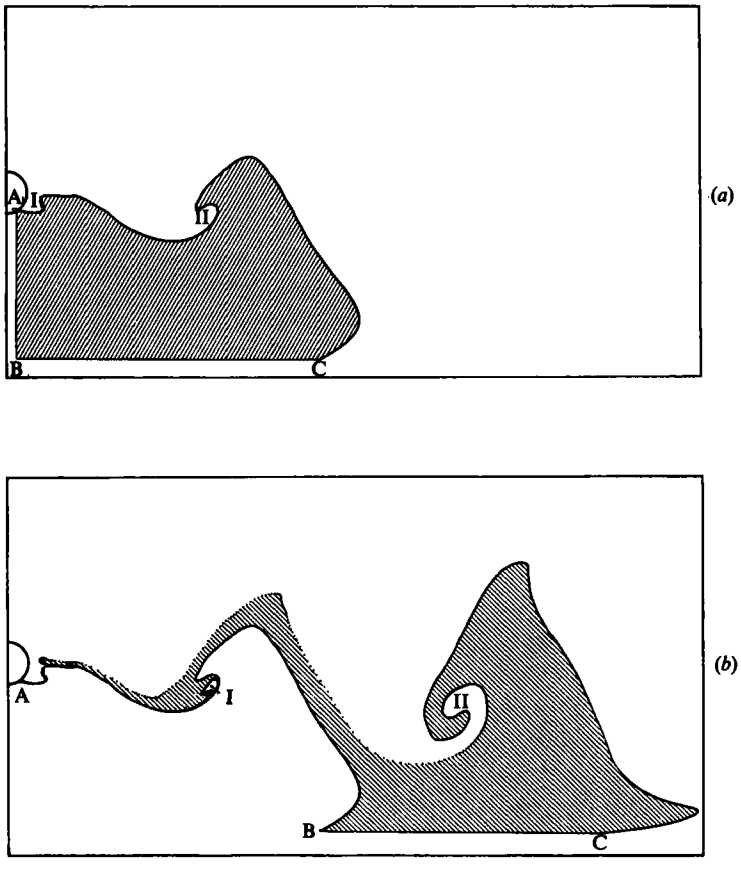

FIGURE 13. Material elements in the wake. The fluid indicated by the hatched area in (*a*) occupies the hatched area in (*b*) one period later.

point C in one period. The line stretches a great deal as it moves; AC is about four times as long as AB.

The vorticity balance on the material element in figure 13(*a*) is performed in the following way. First, the amount of vorticity (ω) carried into the element by the fluid flowing past the line AB was computed by evaluating the integral

$$\int_0^T \int_A^B u\omega \, \mathrm{d}y \, \mathrm{d}t.$$

Next, the amount of vorticity contained in the element is obtained by evaluating the contour integral for the circulation, i.e.

$$\oint_{ABCA} \boldsymbol{u} \cdot \mathrm{d}\boldsymbol{r}.$$

where $\boldsymbol{u}$ is the vector velocity and $\mathrm{d}\boldsymbol{r}$ is a position vector. Both the circulation integral and the advective flux integral are evaluated using second-order trapezoid rule formulas. Table 2, which summarizes the results of the vorticity balance, shows that only 11% of the vorticity shed from the cylinder in one period is cancelled during that period.

Dimensionless vorticity shed from one side of a cylinder during one period:

$$\frac{1}{DV}\int_0^{\tau}\int_A^B u\omega \,\mathrm{d}y\,\mathrm{d}t = 5.98$$

Contour ABCA evaluated at	$\frac{1}{DV}\int_{ABCA} \boldsymbol{u}\cdot\mathrm{d}\boldsymbol{r}$	Vorticity lost (%)
τ	5.32	11
2τ	3.59	40

TABLE 2. Vorticity balance in the wake

Continuing the integration of the material lines AB and AC for another period, the fluid is seen to move to the area designated by the hatching in figure 13(*b*). Line AB occupies the same position as the line AC did in figure 13(*a*). The line AC in figure 13(*b*) follows a complicated path because some of the fluid is caught in the recirculation region. Briefly, it follows the path from the point A out to the vortex core marked I, goes counterclockwise around the core and returns towards the cylinder along a path indistinguishable, on the scale of this drawing, from the one returning to the point A. Upon returning to the rear of the cylinder, the path to C continues in a clockwise direction around the hatched 'tongue' of fluid in the recirculation region, and then away from the cylinder along the upper boundary. The vortex core marked I in figure 13(*b*) represents that part of the recirculation region that is shed in a single vortex. It is precisely the body of fluid defined as the vortex core by the use of the bounding streakline in the previous section.

Clearly, as the material element is spread out along the wavy wake centreline, the loss of vorticity due to cancellation will increase. This is substantiated in table 2, which shows that 40 % of the vorticity shed from the cylinder has been lost after two periods in the flow, compared to only 11 % after a single period.

Gerrard (1978) suggested that the apparent transition in the vortex-shedding mechanism at $Re = 100$ could be correlated with a change in the relative importance of diffusive and advective vorticity transport in the recirculation region. This suggests an interesting numerical experiment which could be carried out using the techniques just described to obtain a vorticity balance. If the vorticity balance obtained for a vortex-shedding wake were compared to one obtained for a (physically unstable) steady-state wake at the same Re, a measure of the increase in the loss of vorticity due to advective processes in the wake would be obtained. If this experiment were carried out over a range of Reynolds numbers, a change in the relationship between this measure and the Reynolds number in the vicinity of $Re = 100$ would support Gerrard's hypothesis.

8. Conclusion

Computer-aided flow-visualization techniques were used to produce streamline, streakline and material-line representations in a vortex-shedding flow field. The wake was characterized in a manner analogous to that used at lower Reynolds numbers in steady wakes by describing the trajectories of critical points associated with the instantaneous streamlines. Interestingly, these trajectories seem to be a sensitive indicator of the quality of the numerical simulation. For the finite-element simulation

analysed herein, the magnitudes of the discontinuities in these trajectories indicate the need for mesh refinement in the near-wake region.

The vortex-shedding mechanism at $Re = 110$ predicted by the two-dimensional Navier–Stokes model was verified by demonstrating its agreement with the experimental streakline results of Gerrard (1978). A result of particular interest is that the fluid from one side of the cylinder, which is entrained in the recirculation region, spends about one period there before being shed into the wake in a vortex originating on the same side of the wake. This observation is in disagreement with the experimental findings of Zdravkovich (1969), and leads one to speculate that the vortex-shedding mechanism is sensitive to the turbulence level of the free stream.

The following physical description of a vortex and the initiation of the shedding process was indicated by analysis of the streamline and streakline visualizations. A vortex core consists of fluid that is injected into the wake from the recirculation region. A core is bounded by the streakline that originates near the rear separation point on the side from which the vortex is shed. The initiation of the shedding process is indicated by the first appearance of a bulge in the bounding streakline where the fluid is to be injected into the wake. The time at which this bulge occurs corresponds to the transition in the streamline patterns from having an alleyway drawing fluid from the side of the cylinder that is about to shed the vortex, to having an alleyway drawing fluid from the opposite side.

A general technique for doing a vorticity balance by following material elements of fluid through the flow field was presented. From this it was determined that, of the vorticity shed from the cylinder in one period, 11 % of it is lost by diffusion into oppositely signed vorticity during that period. Further, after two periods the amount lost increases to 40 %. By contrast, the traditional method of doing a vorticity balance by fitting a vortex model to the observed velocity distribution in the wake gives the result that 60 % of the vorticity is lost (Berger & Wille 1972). Two possible explanations are offered for the difference between the results of the two techniques. One is that the vortex models do not adequately account for the vorticity distribution in a low-Reynolds-number wake. The second is that the wakes studied using the traditional models were exhibiting a vortex-shedding mechanism similar to that observed by Zdravkovich; hence the vorticity loss was greater owing to fluid from one side of the wake being entrained into vortices shed from the opposite side.

The author gratefully acknowledges that this work was made possible by the grant of a National Research Council/National Bureau of Standards Post-doctoral Research Associateship.

Appendix

Particle trajectories are obtained by numerical solution of the system of equations

$$\left.\begin{aligned} \dot{x} &= u(x(\xi,\eta), y(\xi,\eta), t) = \sum_{i=1}^{N} u_i(t)\,\phi_i(\xi,\eta), \\ \dot{y} &= v(x(\xi,\eta), y(\xi,\eta), t) = \sum_{i=1}^{N} v_i(t)\,\phi_i(\xi,\eta), \end{aligned}\right\} \tag{A 1}$$

where $\dot{x}, \dot{y}$ are total derivatives of x, y with respect to time; ξ, η are the local coordinates on the reference element; u_i, v_i are the nodal values of the velocity components; ϕ_i are the biquadratic basis functions on the reference element; and N

is the number of degrees of freedom in the basis set on an element. The relationship between the local coordinates ξ, η and the global coordinates x, y are given by the isoparametric mapping

$$\left.\begin{aligned} x(\xi,\eta) &= \sum_{i=1}^{N} x_i \phi_i(\xi,\eta), \\ y(\xi,\eta) &= \sum_{i=1}^{N} y_i \phi_i(\xi,\eta). \end{aligned}\right\} \tag{A 2}$$

Because (A 1) has ξ, η as the independent variables an approach to computing the particle trajectories using these variables (i.e. $\xi(t), \eta(t)$) was employed. Thus the position of a particle in the grid is represented by three coordinates: the element number, ξ and η.

The integration scheme is based on a Taylor series expansion. The motion of a particle with initial position ξ_i, η_i is given by

$$\left.\begin{aligned} \xi_{i+1} &= \xi_i + \Delta t \dot{\xi}_i + \tfrac{1}{2}\Delta t^2 \ddot{\xi}_i + \ldots, \\ \eta_{i+1} &= \eta_i + \Delta t \dot{\eta}_i + \tfrac{1}{2}\Delta t^2 \ddot{\eta}_i + \ldots, \end{aligned}\right\} \tag{A 3}$$

where the dots refer to total time derivatives. The order of the scheme is determined by the highest-order term retained in (A 3). Chain-rule differentiation leads to the following linear systems which are solved by Crammer's rule for the required derivatives:

$$\begin{bmatrix} x_\xi & x_\eta \\ y_\xi & y_\eta \end{bmatrix} \begin{bmatrix} \dot{\xi} \\ \dot{\eta} \end{bmatrix} = \begin{bmatrix} u \\ v \end{bmatrix}, \tag{A 4}$$

and

$$\begin{bmatrix} x_\xi & x_\eta \\ y_\xi & y_\eta \end{bmatrix} \begin{bmatrix} \ddot{\xi} \\ \ddot{\eta} \end{bmatrix} = \begin{bmatrix} \dot{u} - (x_{\xi\xi}\dot{\xi}^2 + 2x_{\xi\eta}\dot{\xi}\dot{\eta} + x_{\eta\eta}\dot{\eta}^2) \\ \dot{v} - (y_{\xi\xi}\dot{\xi}^2 + 2y_{\xi\eta}\dot{\xi}\dot{\eta} + y_{\eta\eta}\dot{\eta}^2) \end{bmatrix}. \tag{A 5}$$

The notation x_ξ denotes the partial derivative of x with respect to ξ and is obtained by differentiating (A 2). The derivatives of the basis functions ϕ_i with respect to ξ and η (i.e. $\phi_{i,\xi}, \phi_{i,\eta}, \phi_{i,\xi\xi}$, etc.) are obtained analytically. The total time derivatives $\dot{u}$ and $\dot{v}$ are

$$\left.\begin{aligned} \dot{u} &= u_t + uu_x + vu_y, \\ \dot{v} &= v_t + uv_x + vv_y. \end{aligned}\right\} \tag{A 6}$$

The partial time derivatives u_t and v_t were computed and saved as the finite-element solution was generated. They are represented as

$$\left.\begin{aligned} u_t &= \sum_{i=1}^{N} u_{i,t}\phi_i(\xi,\eta), \\ v_t &= \sum_{i=1}^{N} v_{i,t}\phi_i(\xi,\eta), \end{aligned}\right\} \tag{A 7}$$

where $u_{i,t}, v_{i,t}$ are the nodal values of u_t, v_t. The spatial derivatives of the velocity are obtained by differentiating (A 1), and the spatial derivatives of the ϕ_i (i.e. $\phi_{i,x}, \phi_{i,y}$) are obtained from the linear system

$$\begin{bmatrix} x_\xi & y_\xi \\ x_\eta & y_\eta \end{bmatrix} \begin{bmatrix} \phi_{i,x} \\ \phi_{i,y} \end{bmatrix} = \begin{bmatrix} \phi_{i,\xi} \\ \phi_{i,\eta} \end{bmatrix}. \tag{A 8}$$

Equations (A 1)–(A 8) describe how particles are moved within a single element. When a particle passes from one element to another, the integration for a single timestep must be stopped as a boundary is encountered, and new values of $\dot{\xi}$, $\dot{\eta}$, $\ddot{\xi}$ and $\ddot{\eta}$ must be calculated for the new element before completing the timestep. This is because the Jacobian of the mapping, from physical space to the reference element, may be discontinuous at inter-element boundaries. Since the reference element is defined on the region $-1 \leqslant \xi, \eta \leqslant 1$, determining when the particle leaves an element is trivial. Determining which element the particle enters, and through which local side, requires searching the nodal connection array. Since this will have to be done many times throughout the course of a streakline or streamline calculation, it is efficient to perform a 'preprocessing' step in which arrays are constructed which contain, for each element in the grid, the element numbers for those elements bounding it on each side, and the local side numbers of the neighbouring elements. Then, when a particle enters a new element, its local coordinates on the boundary of the new element can be quickly determined.

It should also be pointed out that the computational efficiency can be increased by taking advantage of the fact that a properly designed mesh will employ the full isoparametric mapping only for those boundary elements on curved surfaces where it is required. All interior elements and boundary elements with straight sides should employ a linear mapping, which simplifies (A 2) and all subsequent derivatives of it.

REFERENCES

Bearman, P. W. & Graham, J. M. R. 1980 Vortex shedding from bluff bodies in oscillatory flow: a report on Euromech 119. *J. Fluid Mech.* **99**, 225–245.

Berger, E. & Wille, R. 1972 Periodic flow phenomena. *Ann. Rev. Fluid Mech.* **4**, 313–340.

Birkhoff, G. & Zarantonello, E. H. 1957 *Jets, Wakes, and Cavities*, chap. 13. Academic.

Bloor, M. S. & Gerrard, J. H. 1966 Measurements on turbulent vortices in a cylinder wake. *Proc. R. Soc. Lond.* A **294**, 319–342.

Bouard, R. & Coutanceau, M. 1980 The early stage of development of the wake behind an impulsively started cylinder for $40 < Re < 10^4$. *J. Fluid Mech.* **101**, 583–607.

Coutanceau, M. & Bouard, R. 1977*a* Experimental determination of the main features of the viscous flow in the wake of a circular cylinder in uniform translation. Part 1. Steady flow. *J. Fluid Mech.* **79**, 231–256.

Coutanceau, M. & Bouard, R. 1977*b* Experimental determination of the main features of the viscous flow in the wake of a circular cylinder in uniform translation. Part 2. Unsteady flow. *J. Fluid Mech.* **79**, 257–272.

Eaton, B. E. 1983 The Galerkin finite element method applied to viscous incompressible flows. Ph.D. thesis, University of Colorado.

Engelman, M. S., Sani, R. L., Gresho, P. M. & Bercovier, M. 1982 Consistent *vs.* reduced integration penalty methods for incompressible media using several old and new elements. *Intl J. Num. Meth. Fluids* **2**, 25–42.

Gerrard, J. H. 1978 The wakes of cylindrical bluff bodies at low Reynolds number. *Phil. Trans. R. Soc. Lond.* A **288**, 351–382.

Gresho, P. M., Chan, S. T., Lee, R. L. & Upson, C. D. 1984 A modified finite element method for solving the time-dependent, incompressible Navier–Stokes equations. Part 2: Applications. *Intl J. Num. Meth. Fluids* **4**, 619–640.

Gresho, P. M., Lee, R. L. & Sani, R. L. 1980 On the time dependent solution of the incompressible Navier–Stokes equations in two and three dimensions. In *Recent Advances in Numerical Methods in Fluids* (ed. C. Taylor & K. Morgan). Swansea: Pineridge.

Perry, A. E., Chong, M. S. & Lim, T. T. 1982 The vortex-shedding process behind two-dimensional bluff bodies. *J. Fluid Mech.* **116**, 77–90.

SANI, R. L., EATON, B. E., GRESHO, P. M., LEE, R. L. & CHAN, S. T. 1981 On the solution of the time-dependent incompressible Navier–Stokes equations via a penalty Galerkin finite element method. *Presented at the Intl Conf. on Num. Meth. for Laminar and Turbulent Flow, Venice, Italy, July 1981.*

TRITTON, D. J. 1959 Experiments on the flow past a circular cylinder at low Reynolds numbers. *J. Fluid Mech.* **6**, 547–567.

ZDRAVKOVICH, M. M. 1969 Smoke observations of the formation of a Kármán vortex street. *J. Fluid Mech.* **37**, 491–496.